Journal of Manufacturing Processes
Vol. 3/No. 1
2001

Cooling Effects in Multiscan Laser Forming

Jin Cheng and **Y. Lawrence Yao,** Dept. of Mechanical Engineering, Columbia University, New York, New York, USA

Abstract

For laser forming of sheet metal to become a practical production or rapid prototyping tool, multiple scans of the workpiece with the laser are necessary to achieve the required magnitude of deformation. Between consecutive scans, substantial waiting time is normally necessary for the workpiece to cool down so that a steep temperature gradient can be reestablished in the next scan. This paper first experimentally and numerically examines the effect of forced cooling on single-scan laser forming processes. Cooling effects under various conditions, including different laser power, scanning speed, nozzle offset, and cooling air pressure, are investigated. Cooling effects on microstructure change and other mechanical properties, including strength, ductility, and hardness, are also examined. A focus is to investigate the cooling effect on the deformation mechanism, including competing effects on temperature and flow stress. The investigation on multiscan laser forming shows forced cooling has the potential to significantly reduce the total forming time while having no undesirable effects on microstructure change and other mechanical behavior. Cooling in the buckling mechanism dominated laser forming process is also considered. The established numerical model for laser forming with forced cooling provides greater insights into the cooling effects on the deformation mechanism, helps predict such effects on final dimensional accuracy and mechanical properties, and can be extended to optimize the multiscan laser forming process.

Keywords: *Laser Forming, Forced Cooling, Finite Element Method, Microstructure, Rapid Prototyping*

Introduction

Laser forming involves a laser-induced thermal distortion to shape sheet metal without hard tooling or external forces. Compared with the traditional metal forming technologies, laser forming has many advantages: the cost of the forming process is greatly reduced because no tools or external forces are involved, and laser forming is useful for small batch production and a high variety of sheet metal components. With the high flexibility in the laser beam's delivery and power regulating systems, it is easy to incorporate laser forming into an automatic flexible manufacturing system. Laser forming uses localized heating to induce controlled deformation and therefore has the advantage of energy efficiency as compared to other thermal processes where an entire workpiece normally needs to be heated.

Despite of these advantages, progress needs to be made for laser forming to become a practical processing technology. For instance, to create more practical, three-dimensional shapes, multiple laser scans are necessary to obtain the required magnitude of deformation; a single scan only gives a limited amount of deformation. If the workpiece is not cooled sufficiently close to room temperature after a scan, the temperature gradient required in laser forming may not be readily reestablished in the next scan. In addition, the aggregated heat may result in surface melting. However, the waiting time between scans can be significant if there is no forced cooling.

Sprenger et al.[1] extensively investigated multiscan laser forming. They showed that the decrease of absorption coefficient, the increase of the sheet thickness, and work hardening of the material affect the degressive courses of bending angle with increasing number of irradiations. However, Sprenger et al. did not address the cooling issue. Odumodu and Das[2] suggested to use forced cooling in multiscan laser forming but did not investigate its effects. Hennige and Geiger[3] have experimentally investigated cooling in multiscan laser forming of aluminum sheets. They suggested high-pressure air cooling and passive and active water cooling and showed that, compared with air cooling, active water cooling reduces the entire processing time by increasing the bend angle per scan. Hennige and Geiger also showed that both air cooling and water cooling have no detrimental effects on the microstructure of the formed parts. Although it was shown that active water cooling is more efficient, it is inconvenient in industrial settings. Moreover, water cooling complicates the process by introducing laser-liquid-solid interactions and requires an additional liquid container and circulation system.

Although only limited investigations have been conducted in the experimental and computer modeling of the laser forming process with forced cooling,

cooling has long been used in other thermal manufacturing processes for various reasons, and a great deal of experience and research results have been accumulated, from which the present work draws. For example, after hot rolling, deformation problems caused by nonuniform temperature distribution in asymmetrical ship profiles can be solved by selective water spray cooling. Olden, Smabrekke, and Raudensky[4] carried out experiments to obtain the correct heat conditions and applied them to a 2-D numerical model to simulate the selective air/water spray cooling effect. Debray, Teracher, and Jonas[5] investigated the microstructure and mechanical properties of C-Mn ferrite-bainite steel over a wide range of cooling rates and cooling temperatures in hot rolling. The advantages of air-cooled steels include the elimination of heat treatment, reduced distortion, improved machinability, and more consistent properties. In forging operations, cooling has been controlled accurately and reliably, enabling the required mechanical properties to be imparted without additional heat treatment.[6]

This paper presents experimental and numerical investigations aimed at gaining better understanding of cooling effects in single and multiscan laser forming. Experimentally validated numerical results provide greater insights into cooling effects on deformation characteristics, temperature profile, stress distribution, and process efficiency. Cooling effects on microstructure and other mechanical properties are also examined. These results help predict such effects on final dimensional accuracy and mechanical properties.

Forming Process with Forced Cooling

The following general assumptions have been made. The workpiece material is isotropic, has constant density, and is opaque; that is, the laser beam does not penetrate appreciably into the solid. The power density distribution of the laser beam follows a Gaussian function. The laser operates in continuous wave (CW) mode. Material properties such as the modulus of elasticity, heat transfer properties, thermal conductivity, specific heat, and flow stress are temperature dependent. The rate of deformation is the total strain rate that is the sum of the viscous, elastic, and plastic strain rate. A strain-hardening coefficient, which is also temperature dependent, is defined to consider strain hardening of the material.

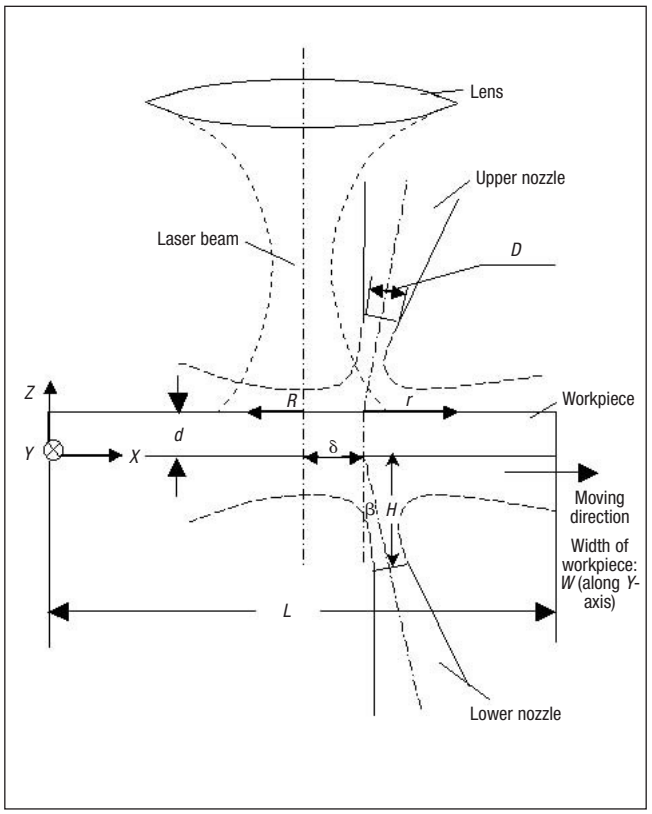

Figure 1
Laser Forming System with Cooling Jets

Energy dissipated through plastic deformation is negligible compared with the intensive laser energy involved. No melting is involved in the forming process. Finally, no external forces are applied to the solid. Stresses occur only due to thermal expansion or contraction.

Heat Transfer. The transient conduction for a solid workpiece of dimension L by W by d (*Figure 1*), radiated by a laser beam can be expressed in terms of temperature as:

$$\rho c_p \frac{\partial T}{\partial t} = \nabla \cdot (k \nabla T) \tag{1}$$

subject to the boundary conditions: $y = 0$: $T \rightarrow T_\infty$; $y = W$: $T \rightarrow T_\infty$; $z = 0$: $\alpha_{abs} F \cdot \hat{n} = -\hat{n} \cdot (k \nabla T)$, $Q_{conv} = h_{z=0} (T - T_\infty)$, and $Q_{rad} = \varepsilon \sigma (T^4 - T^4_\infty)$; $z = d$: $Q_{conv} = h_{z=H} (T - T_\infty)$, and appropriate initial conditions such as $t = 0$: $T(x, y, z, 0) = T_\infty$ where ρ, c_p, k, and α_{abs} are the density, specific heat, thermal conductivity, and the material's absorbency, respectively. The symbols x, y, and z are the Cartesian coordinates (*Figure 1*); $\hat{n}$ is the unit vector normal to the surface pointing

to the solid; Q_{rad} and Q_{conv} are the heat flux due to the radiation and convection, respectively. The heat transfer coefficient due to the impinging jet on the top and bottom surface of the solid are $h_{z=0}$ and $h_{z=d}$, respectively; ε and σ are the emissivity and Stefan-Boltzmann constant, respectively. T is the temperature of the plate and T_∞ is the ambient temperature.

The heat flux due to the Gaussian laser power is expressed as:

$$F = Q_{\max} \exp\left(-R_k R^2\right) \text{and } Q_{\max} = P_{laser} R_k / \pi \tag{2}$$

where Q_{max} is the heat flux intensity of the laser beam, R is the distance to the laser beam center, R_k is the concentration coefficient, and P_{laser} is the laser power.

Heat Convection Due to the Cooling Jet(s). Simple converging nozzles with circular cross section are assumed. The following equations correlate the integral mean values[7]

$$\left(\frac{\overline{Nu}}{\Pr^{0.42}}\right)_{SRN} = \frac{D}{R}\frac{1-1.1D/r}{1+0.1(H/D-6)D/r}F(\mathrm{Re}) \tag{3}$$

for $2.5 \le r/D \le 7.5$

$$\left(\frac{\overline{Nu}}{\Pr^{0.42}}\right)_{SRN} = F_1(\mathrm{Re}, r/D)k(H/D, r/D) \tag{4}$$

for $0 \le r/D \le 2.5$

where *Re*, *Nu*, and *Pr* are the Reynolds, Nusselt, and Prandtl number, respectively, H is the vertical distance of the nozzle to the sheet surface, D is the diameter of the nozzle, and r the radial distance from the nozzle center. The above equations are valid for $2{,}000 \le Re \le 4{,}000{,}000$ and $2 \le H/D \le 12$. The function $F(Re)$ may be represented by the following smooth curve expression

$$F(\mathrm{Re}) = 2\,\mathrm{Re}^{1/2}\left(1+\frac{\mathrm{Re}^{0.55}}{200}\right)^{0.5} \tag{5}$$

F_1 $(Re, r/D)$ and k $(H/D, r/D)$ are represented graphically. For the experiments reported in this paper, the Reynolds number ranges from 1×10^6 to 4×10^6 around the stagnation point.

The angle of incidence of the jet relative to the impinged surface relocates the point of maximum heat transfer and reduces the heat transfer rate, but the average heat transfer coefficient remains essentially unchanged. Perry[8] concluded that the stagnation heat transfer coefficient decreases as the angle of incidence is reduced from 90 degrees. The total heat transfer rate, however, remains nearly constant, because the effective surface area in contact with a given jet increases as the angle decreases. For the present study, the angle of incidence remained less than 10 degrees away from the vertical position and therefore its effect is neglected.

Thermal Stress. Assume the faces ($Z = 0$ and d) of the workpiece plate are free of traction; that is, $\underline{\underline{\sigma}} \cdot \hat{n} = 0$ and the edges ($x = 0$, $y = 0$, $x = L$, $y = W$) have no traction and no clamped boundary conditions (*Figure 1*). The plate is initially free of stress. Because the initial stress distribution is prescribed, it may be integrated forward in time to obtain the unique stress distribution for all times. Under the conditions given by the heat transfer portion, the stress and strain distribution is solved using the following sets of equations.

Because there are no external forces, body forces and acceleration components, the entire stress distribution of the part obeys $\nabla \cdot \sigma = 0$, or

$$\frac{\partial \sigma_{ij}}{\partial x_j} = 0 \tag{6}$$

The relationship between the state of stress in the plate at time t, the state of strain in the plate at time t and the rate of change of the prescribed temperature distribution at that time follows. The total strain rate $\dot{\varepsilon}_{ij}$ is composed of the mean strain rate $\dot{\varepsilon}_{kk}$ and the deviatoric strain rate $\dot{e}_{ij}$. The mean strain rate is given by

$$\dot{\varepsilon}_{kk} = \frac{1-2\nu}{3E}\dot{\sigma}_{kk} + \alpha\dot{T} \tag{7}$$

where E is Young's modulus, ν is the Poisson's ratio, σ_{kk} is the mean stress, and α is the heat expansion coefficient. For laser forming processes at high stress and temperature levels, the viscoelastic effect may both be significant. Thus, the deviatoric strain e_{ij}, which is composed of an elastic portion e^E_{ij}, a viscoelastic portion e^v_{ij}, and a plastic portion e^P_{ij}, can be written as

$$\dot{e}_{ij} = \dot{e}_{ij}^{E} + \dot{e}_{ij}^{V} + \dot{e}_{ij}^{P} \tag{8}$$

where

$$\dot{e}_{ij}^{E} = \frac{1}{2\mu}\dot{s}_{ij} \text{ and } \dot{e}_{ij}^{v} = \frac{1}{2\eta}s_{ij} \tag{9}$$

where μ is the shear modulus, η is the viscosity constant, and s_{ij} the deviatoric stress component. e^{P}_{ij} is assumed to be governed by flow rules associated with perfectly plastic behavior and the von Mises yield criterion, that is,

$$\begin{aligned} &e_{ij}^{P} = 0 \\ &\text{if } \frac{1}{2}s_{ij} < k^2(T), \text{ or if } \frac{1}{2}s_{ij} = k^2(T) \text{ and} \\ &s_{ij}\dot{s}_{ij} - 2kk'\dot{T} \le 0 \\ &e_{ij}^{P} = \lambda s_{ij} \\ &\text{if } \frac{1}{2}s_{ij} = k^2(T) \text{ and } s_{ij}\dot{s}_{ij} - 2kk'\dot{T} \ge 0 \end{aligned} \tag{10}$$

where $\dot{s}_{ij}^{v} = 2\mu\left(\dot{e}_{ij} - \dot{e}_{ij}^{v}\right)$. s^{v}_{ij} is computed as though no plastic flow has occurred, although account is taken of the viscous flow. $k(T)$ is the von Mises yield stress as a function of temperature. A function $g(x,t)$ is introduced, which is zero in the plastic state and unity elsewhere, that is,

$$\begin{aligned} &g(x,t) = 1 \\ &\text{if } \frac{1}{2}s_{ij} < k^2(T), \text{ or if } \frac{1}{2}s_{ij} = k^2(T) \text{ and} \\ &s_{ij}\dot{s}_{ij} - 2kk'\dot{T} \le 0 \\ &g(x,t) = 0 \\ &\text{if } \frac{1}{2}s_{ij} = k^2(T) \text{ and } s_{ij}\dot{s}_{ij} - 2kk'\dot{T} \ge 0 \end{aligned} \tag{11}$$

Therefore, the combined stress-strain relations from Eqs. (8) to (10) can be written as[9]

$$\begin{aligned} \dot{\varepsilon}_{ij} = &\frac{1+\nu}{E}\dot{\sigma}_{ij} - \delta_{ij}\frac{\nu}{E}\dot{\sigma}_{KK} \\ &+\left(\frac{1}{2\eta} + 2(1-g)\lambda\right)\left(\sigma_{ij} - \delta_{ij}\frac{\sigma_{kk}}{3}\right) + \delta_{ij}\alpha\dot{T} \end{aligned} \tag{12}$$

Numerical Simulation. Because the heat transfer and viscoelastic/plastic deformation are symmetric about the vertical plane containing the scanning path, only half of the plate is modeled in the numerical simulation. The symmetric plane is assumed to be adiabatic. The same mesh model is used for the heat transfer analysis and structural analysis. Two adjacent points in the middle of the symmetric plane are assumed to be fixed to remove the rigid body motion. All other points within the symmetric plane are assumed to move only within the symmetric plane throughout the deformation process. A commercial code, ABAQUS, is used to solve the heat transfer and structural problem. In structural analysis, the 20-node element, C3D20, has no shear locking, no hourglass effect, and is thus suitable for a bending-deformation-dominated process such as laser forming. On the other hand, the eight-node element suffers from "shear locking" and is therefore not suitable for such a process. To remain compatible with the structural analysis, a 20-node element, DC3D20, is used in heat transfer analysis.

Experiment

Straight-line laser forming with forced air cooling is schematically shown in *Figure 1*. The scanning path is along the *x*-axis, and the direction perpendicular to the scanning path and within the plate is defined as the *y*-axis. The upper cooling nozzle and lower cooling nozzle were considered, although most experiments were done with the lower nozzle only. They had no relative motion with respect to the laser beam. Simple converging nozzles with circular cross section were used. The angle of incidence of the impinging jet relative to the sheet surface, β, was kept close to 90 degrees to create higher convection heat transfer at the stagnation point. The diameter of the nozzle, *D*, is 1.6 mm, and the standoff distance, *H*, is 8 mm. Most experiments were done with zero offset between the impinging jet stagnation point and the laser beam center, although the effect of the offset distance δ was also investigated. The material is low carbon steel, AISI1010, and 80 mm by 80 mm by 0.89 mm in size. To enhance laser absorption by the workpiece, graphite coating is applied to the surface exposed to the laser.

Most experiments use laser power of 400 or 800 W, except one uses varying power from 400 to 800 W. Most experiments use scanning velocity of 25 or 50 mm/s, except one uses velocity varying from 25 to 80 mm/s. Most experiments use air pressure of 80 psi, except one uses pressure varying from 0 to 80

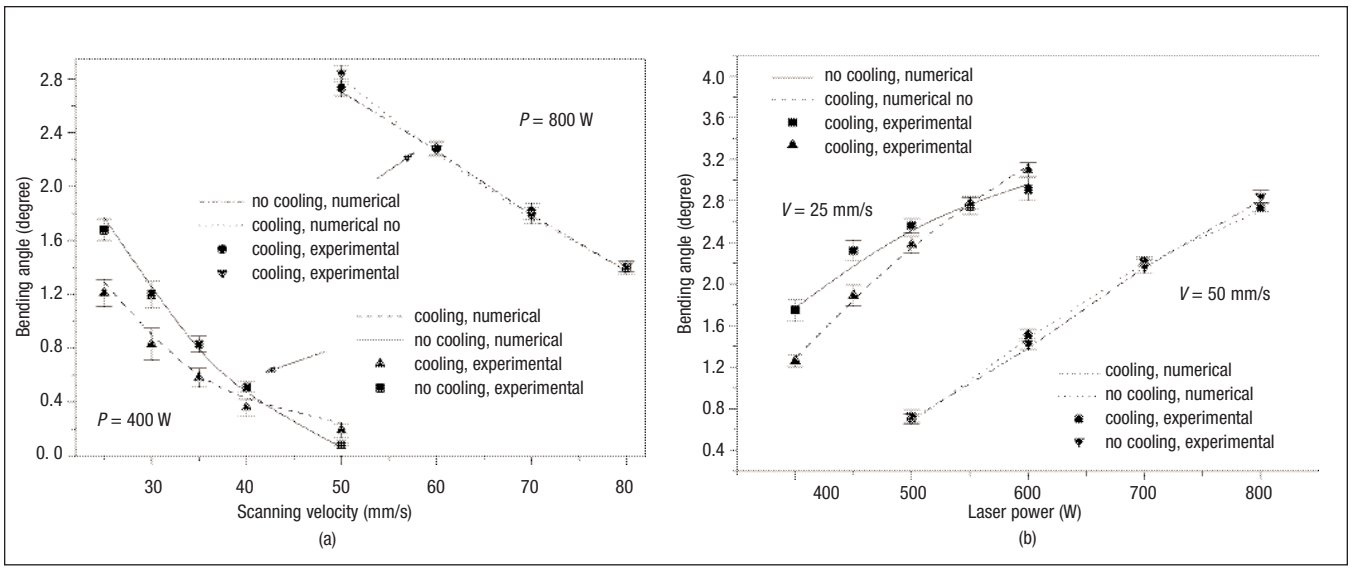

Figure 2
(a) Numerical and experimental bend angle vs. scanning velocity, (b) Numerical and experimental bend angle vs. laser power. (D_{beam} = 4 mm, P_{air} = 80 psi, δ = 0, bottom cooling only)

psi. Most experiments use laser beam size of 4 mm, except one uses 8 mm to induce the buckling mechanism (BM). Most experiments use zero offset, except one uses offset δ varying from 0 to 18 mm. Most experiments use bottom surface cooling only, except one uses top surface cooling and both bottom and top surface cooling. The exact experimental conditions are noted in the figures and their legends.

The laser system used is a PRC-1500 CO_2 laser, which has a maximum output power of 1500 W. A coordinate measuring machine (CMM) is used to measure the bending angle of the formed parts. To calculate the Reynolds number of the air at the nozzle exit that is applied in the numerical simulation, a velocimeter is used to measure the velocity of the air at the nozzle exit. Scanning electronic microscopy is used to investigate the microstructure of the material after laser forming. Tensile test samples are machined by CNC along the scanning path, and tensile tests are conducted on a MTS. A Rockwell hardness tester is used to measure the hardness of the material after laser forming.

Results and Discussion

Simulation Validation and Cooling Effect on Deformation

Figures 2a and *2b* compare simulation and experimental results under a wide range of conditions, and reasonable agreements are seen. *Figure 2a* shows the variation of the bending angle vs. scanning speed with and without cooling. As seen, the bending angle with cooling could be smaller or larger than that without cooling at laser power of 400 W, while there is no appreciable difference between the two at 800 W. To help explain the phenomenon, peak temperature reached at the workpiece top and bottom surfaces as well as corresponding flow stress at these locations are plotted in *Figures 3a* and *3b*. Temperature, work hardening, and strain rate effects were considered in determining the flow stress.

At the lower power of 400 W and lower velocity of 25 mm/s (*Figures 2a* and *3a*), the bending angle with cooling is lower than that without cooling by the greatest margin. Although the bottom-only cooling lowers the bottom temperature significantly (from about 850 K to 700 K) and therefore increases the temperature gradient between the top and bottom surface, which seems to favor more deformation, the cooling at the same time increases the flow stress at the bottom surface quite significantly (from about 120 to 170 MPa). The net result is a decreased bending angle. At the same power but higher velocity of 50 mm/s, the net result is opposite. This is because heat dissipation at this condition is lower due to the shorter cooling time, and the temperature drop at the sample's surfaces is not as great as with the lower scanning speed. As a result, the cooling

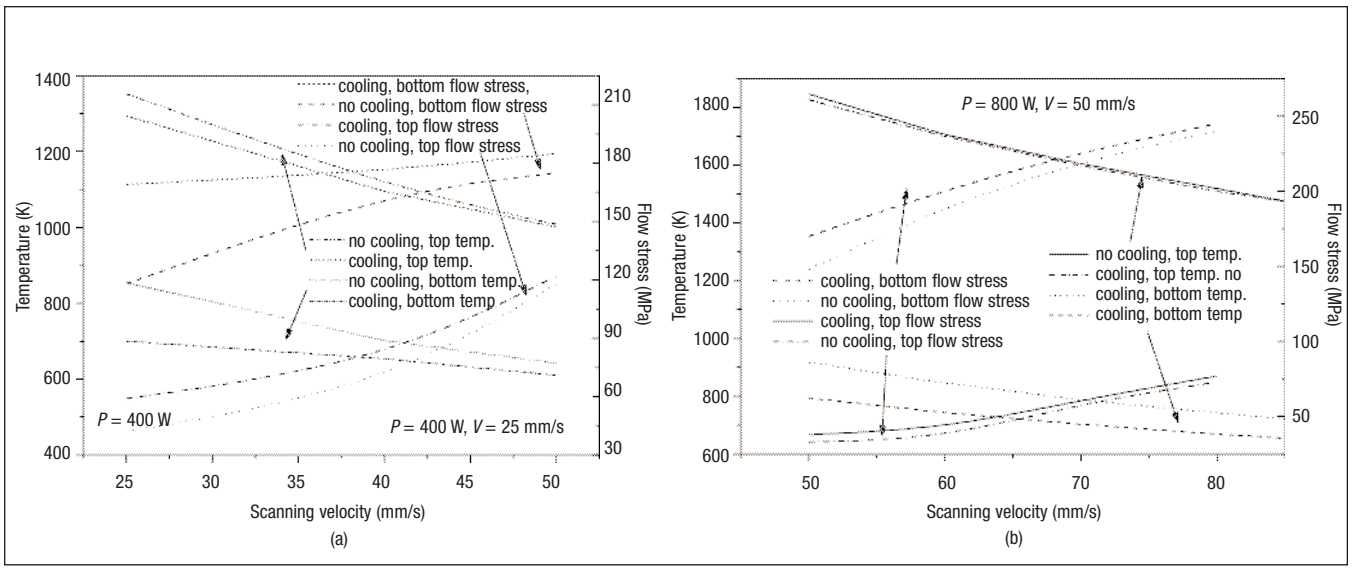

Figure 3
Peak Temperature and Flow Stress
(a) P = 400 W and V = 25 mm/s, (b) P = 800 W and V = 50 mm/s (D_{beam} = 4 mm, P_{air} = 80 psi, δ = 0, bottom cooling only)

effect on temperature gradient increase begins to outweigh the cooling effect on flow stress increase.

At the higher power level of 800 W (*Figures 2a* and *3b*), the cooling effect on bending angle is not significant. A reason is that heat input from the laser is greater and the heat dissipation is relatively lower due to relatively higher velocities. This causes the temperature drop due to the cooling to be lower. As a result, its effect on the flow stress is also lower and the deformation remains largely the same as in the case without cooling. Similar results are obtained when variations of the bending angle are examined against varying laser power while the scanning velocity is kept at constant levels of 25 mm/s and 50 mm/s (*Figures 2b* and *3b*).

Effect of Air Pressure

Figure 4a shows the relationship between the air-cooling pressure and the bending angle under two conditions. When the higher power of 800 W and higher velocity of 50 mm/s is applied, the bending angle increases moderately with air-cooling pressure. This is because under this condition the net heat input into the workpiece is higher, the temperature drop due to the cooling is lower, and therefore the increase in flow stress is also lower. As a result, the temperature gradient increase between the top and bottom surfaces due to air-pressure increase is slightly more dominant. *Figure 4b* shows that the y-axis compressive plastic strain on the top surface only increases slightly when cooling (80 psi) is applied.

When a lower power of 400 W and lower velocity of 25 mm/s is applied, the bending angle decreases as the air-cooling pressure increases. This is because under the condition the net heat input is lower, the temperature drop due to the air cooling is higher, and the increase in flow stress is higher. Although the temperature gradient between the top and bottom surfaces still increases with air pressure, the cooling effect on the flow stress increase becomes dominant when the air pressure increases. This is evident in *Figure 4b* where not only the y-axis compressive plastic strain but also the region of such plastic strain decrease as cooling (80 psi) is applied due to increased flow stress.

Effect of Cooling Nozzle Offset

There exists a time delay between when the top surface reaches its peak temperature and when the bottom surface does due to heat conduction time. Therefore, if the impinging jet is placed coaxially with the laser beam, the cooling may not be the most efficient.

Figure 5 shows the effect of cooling nozzle offset δ (*Figure 1*) on bending angle, where the cases of no cooling and cooling with zero offset are also shown. For the higher power of 800 W and higher velocity of 50 mm/s, the maximal bending angle is obtained

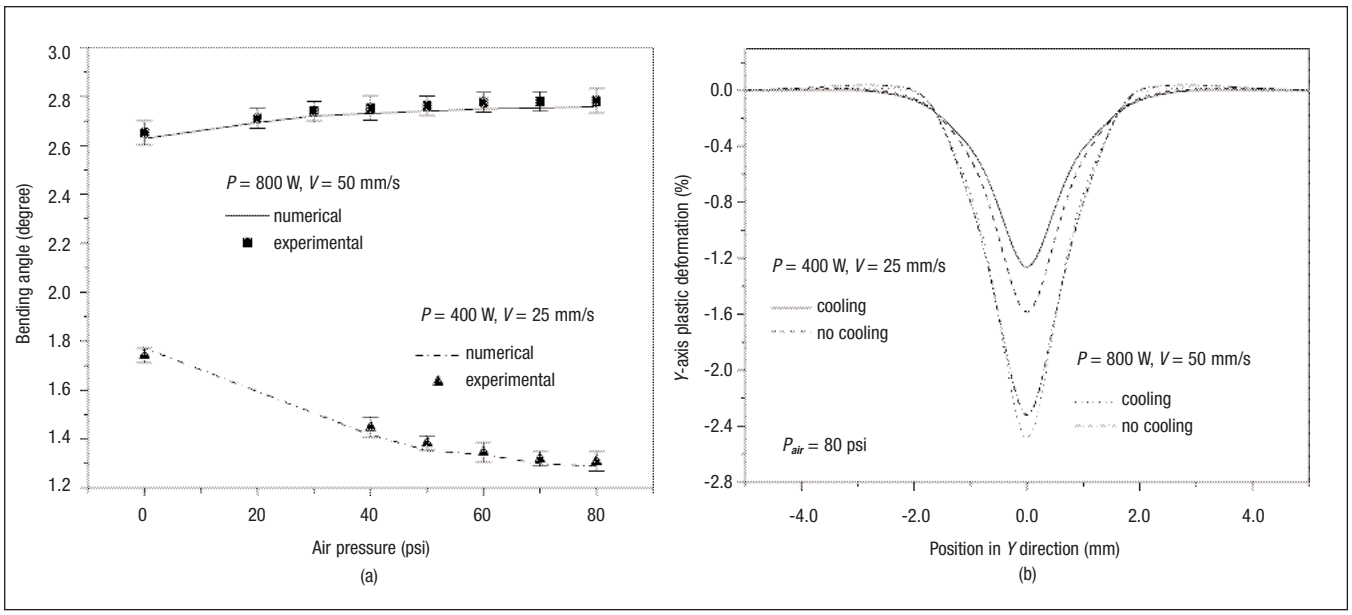

Figure 4
(a) Bend angle vs. air pressure, (b) distribution of *Y*-axis plastic deformation along *Y* direction after laser forming with cooling and without cooling (D_{beam} = 4 mm, δ = 0, bottom cooling only)

when the offset is approximately 5 mm. For the lower power of 400 W and lower velocity of 25 mm/s, the minimal angle (under this condition, cooling causes the bending to decrease, as seen in *Figure 2a*) is obtained at offset about 2 mm. The difference between the two offset values can be easily explained because under the first condition the velocity is twice as that under the second condition; therefore, there is a larger time delay between the top and bottom peak temperature under the first condition.

Microstructure

Grain Structure. *Figure 6a* shows the SEM micrograph of the grain structure of AISI 1010 steel before laser forming. *Figures 7a* and *7b* show the SEM micrographs of the grain structure near the top surface after laser forming with and without cooling. It can be seen that the grain structure is refined after laser forming in both cases. The case with cooling (*Figure 7a*) exhibits a finer grain structure than the one without cooling (*Figure 7b*) obviously because of the higher cooling rate, although in both cases the deformation and peak temperature reached are about the same (*Figures 2b* and *3b*). This is because the nucleation rate of new grains under cooling is higher than that under no cooling condition.

During high-temperature deformation, it is possible to have dynamic recovery and dynamic recrystallization. The ability for a material to do so depends on the stacking fault energy of the material.[10] Materials, such as aluminum alloys and steels, that have a high stacking fault energy do not dynamically recrystallize in a significant way. Therefore, the grain refinement observed above is primarily due to static recovery and static recrystallization taking place after the material is plastically deformed and while it cools down to room temperature. The static

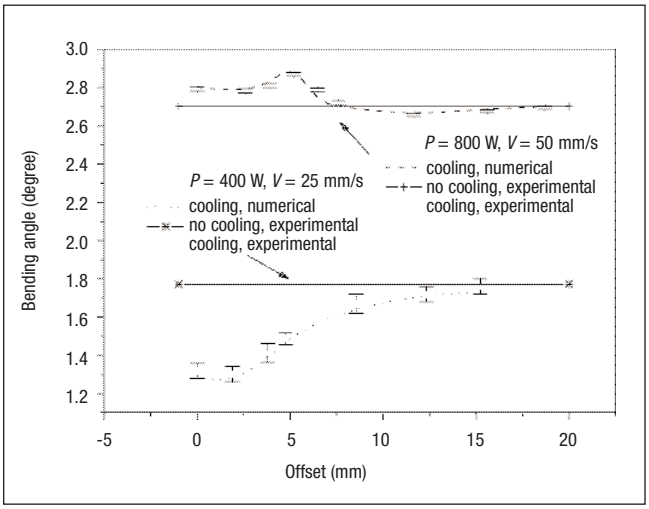

Figure 5
Bend Angle vs. Offset δ
(D_{beam} = 4 mm, P_{air} = 80 psi, δ = 0, bottom cooling only)

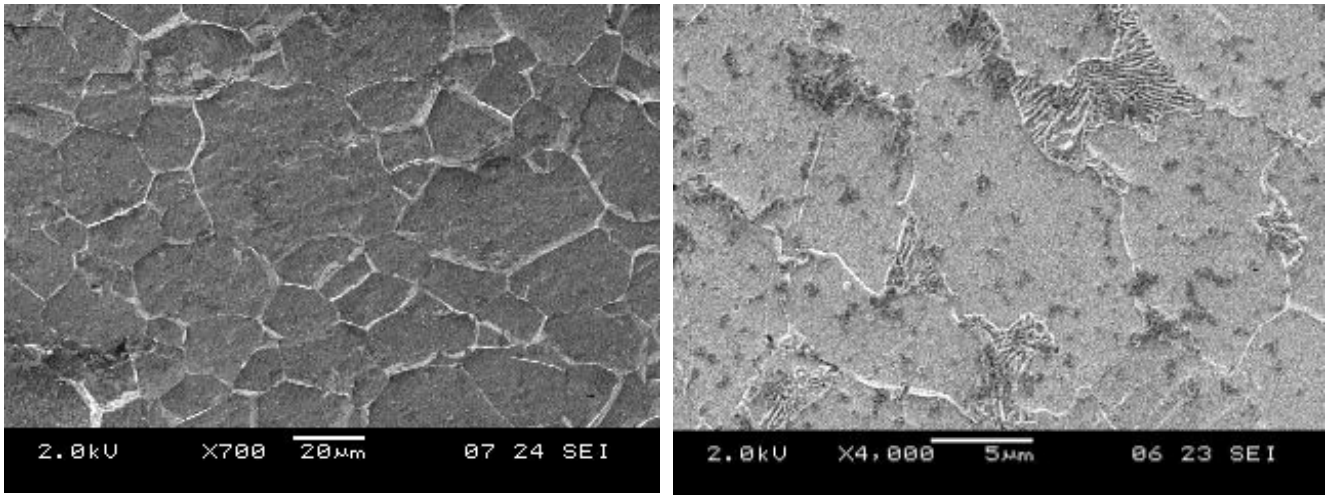

Figure 6
SEM Micrographs of the Raw Material (AISI1010 steel)
(a) low magnification (x700) and (b) high magnification (x4000) showing the phases (ferrite and pearlite)

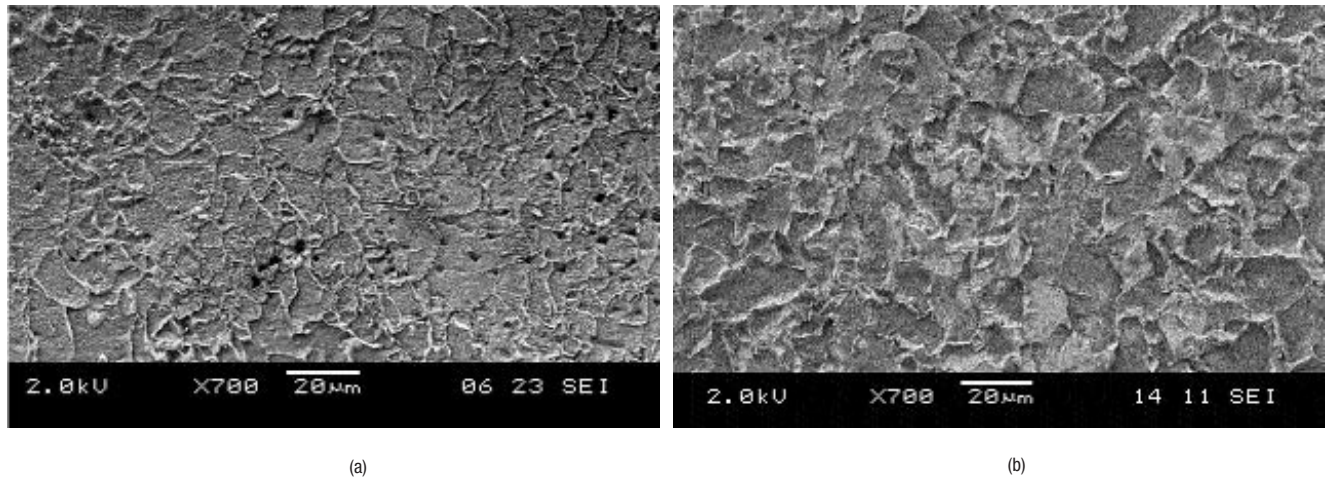

Figure 7
SEM Micrographs of Grain Structure Near Top Surface After Laser Forming
(a) with cooling and (b) without cooling. The grain with cooling is finer. (P = 800 W, V = 50 mm/s, D_{beam} = 4 mm, P_{air} = 80 psi, δ = 0, bottom cooling only)

recrystallization is affected by strain. The greater the strain is, the faster the recrystallization process, and the finer the grain size. Our results show that the grain size at higher laser power (P = 800 W) is finer than at lower laser power (P = 400 W) because the former undergoes larger plastic strain.

Phase Transformation. *Figure 6b* shows the SEM micrograph of the microstructure of the same as-received hypereutectoid steel at a higher magnification (x 4000), under which pearlite with ferrite background can be seen. *Figures 8a* to *8d* show the SEM micrographs near the top and bottom surface after laser forming with and without cooling using the same high magnification. During the transient heating to peak temperature, the material is heated to austenite region. After the material cools down, the

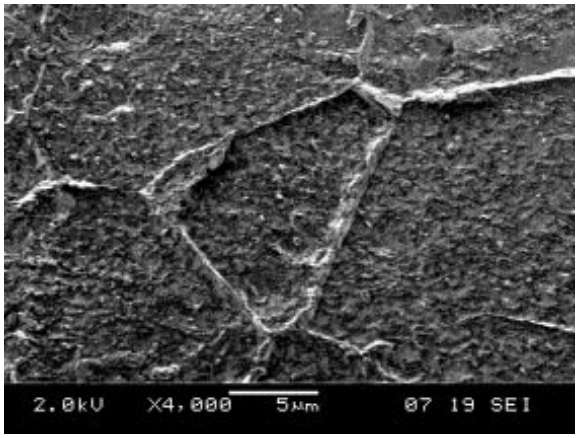

(a) Cooling, top surface

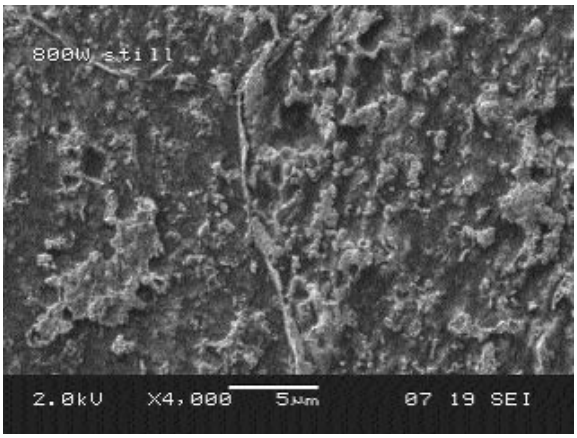

(b) No cooling, top surface

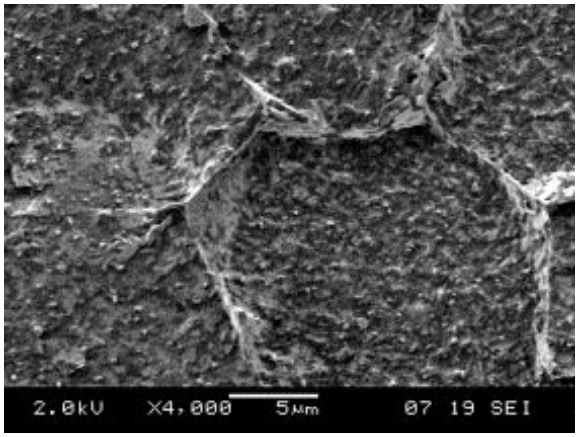

(c) Cooling, bottom surface

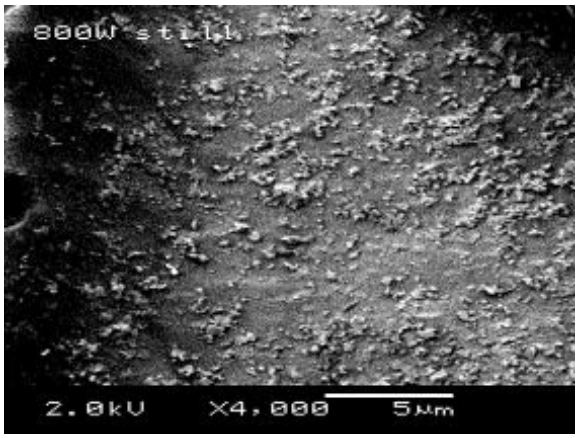

(d) No cooling, bottom surface

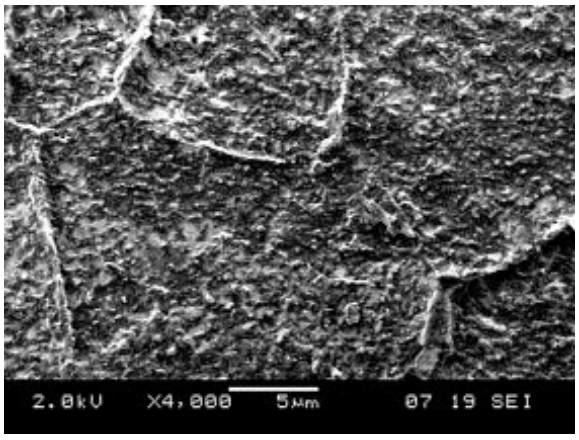

(e) 10 scans, cooling, top surface

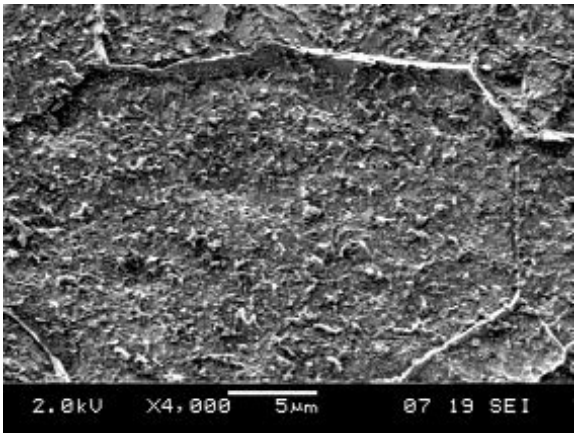

(f) 10 scans, cooling, bottom surface

Figure 8
SEM Micrographs Showing Microstructure of AISI1010 After Laser Forming Under High Magnification (x4000). (a) and (b) after one scan, near top surface with cooling and without cooling, the bainite phase under cooling is finer; (c) and (d) after one scan, near bottom surface with cooling and without cooling, the bainite phase under cooling is finer and volume fraction is higher; (e) and (f) after 10 scans under cooling near top (e) and bottom (f) surfaces. (P = 800 W, V = 50 mm/s, D_{beam} = 4 mm, P_{air} = 80 psi, δ = 0, bottom cooling only)

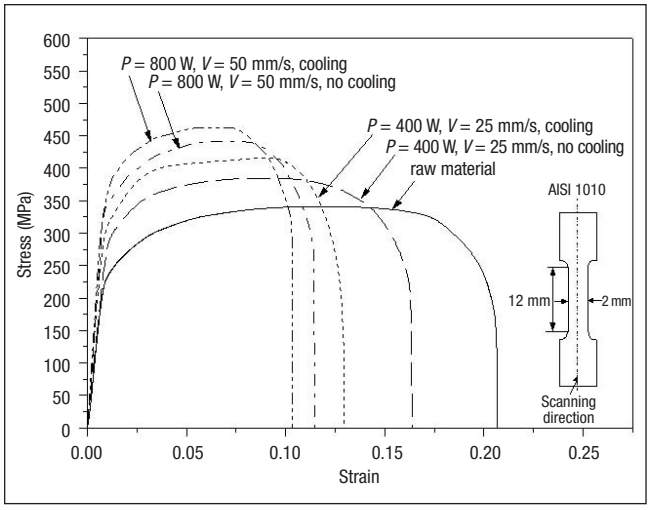

Figure 9
Tensile Stress-Strain Curves of Workpiece Before and After Laser Forming With and Without Cooling (D_{beam} = 4 mm, P_{air} = 80 psi, δ = 0, bottom cooling only).

final phases in the materials contain ferrite, bainite, and perhaps a small amount of pearlite. *Figures 8a* and *8b* show that the microstructure near the top surface after laser forming with cooling contains a more refined bainite phase than that after laser forming without cooling. The bainite nucleates on the ferrite matrix, and the nucleation rate is higher with the high cooling rate.[11] The same phenomenon is observed near the bottom surface, as shown in *Figures 8c* and *8d*.

Mechanical Properties

Figure 9 shows the tensile test results of a laser-formed specimen with and without cooling as compared with raw material. The test length of the specimen is 12 mm and test width is 2 mm, with the laser-scanned region along its axis. It is seen that the yield strength of the material after laser forming is higher than that of the as-received material, the yield strength of the material under laser forming with cooling is higher than that under laser forming without cooling, and the yield strength of the material at higher laser power is higher than that at lower laser power. The reverse can be said about elongation before rupture. As discussed in the previous section, after laser forming the material's grain structure is refined, the material's phase change is from pearlite to refined bainite, and therefore the material is strengthened. The microstructure of materials under cooling shows a finer grain size and a finer bainite phase as compared with no cooling. Therefore, after laser forming, the strength of the material with cooling is higher than without cooling. Comparing the conditions at higher and lower laser power, the former has more plastic deformation and a higher cooling rate and, therefore, a finer grain size.

Figure 10c shows the hardness change due to laser forming and cooling. The hardness of the raw material is about 45 HR. After laser forming, it increases due to strain hardening and grain refinement. With cooling, the hardness increases slightly more.

Multiscan

Figure 10a shows the experimental results of the development of the bend angle as a function of number of scans. The results show approximately linear patterns and indicate that the work hardening effect is offset by the softening effect of the repeated laser scans. Although the resultant bending angles with cooling and without cooling only differ moderately, the total times it takes for the 10 scans to complete are vastly different. Without cooling, a substantial amount of time (in this case, about 150 seconds) has to be waited for the workpiece to cool down to near room temperature to be able to reestablish a steep temperature gradient during the scan that immediately follows. With forced cooling, such a waiting period was reduced to about 10 seconds because the cooling rate with forced cooling is much higher, as seen from the time history of temperature shown in *Figure 10b*. As a result, the total forming time for the 10-pass processes reduced from about 23 minutes without cooling to less than 2 minutes with cooling. This shows cooling has the potential to greatly speed up multiscan operations, which are necessary if laser forming is to become a practical production tool. At the same time, it has been shown that cooling does not have major detrimental effects on deformation efficiency, microstructure, and mechanical properties.

Figure 10c shows the Rockwell hardness test results after multiscan under two different conditions. While the multiscan proceeds, strain hardening and recovery/recrystallization-induced softening coexist and compete with each other. At the higher power of 800 W and higher velocity of 50 mm/s, softening is more dominant due to higher temperature although the deformation is also larger. As a result, the hardness decreases somewhat when more scans are carried out. At the lower power of 400 W and lower velocity of 25 mm/s, the hardening and

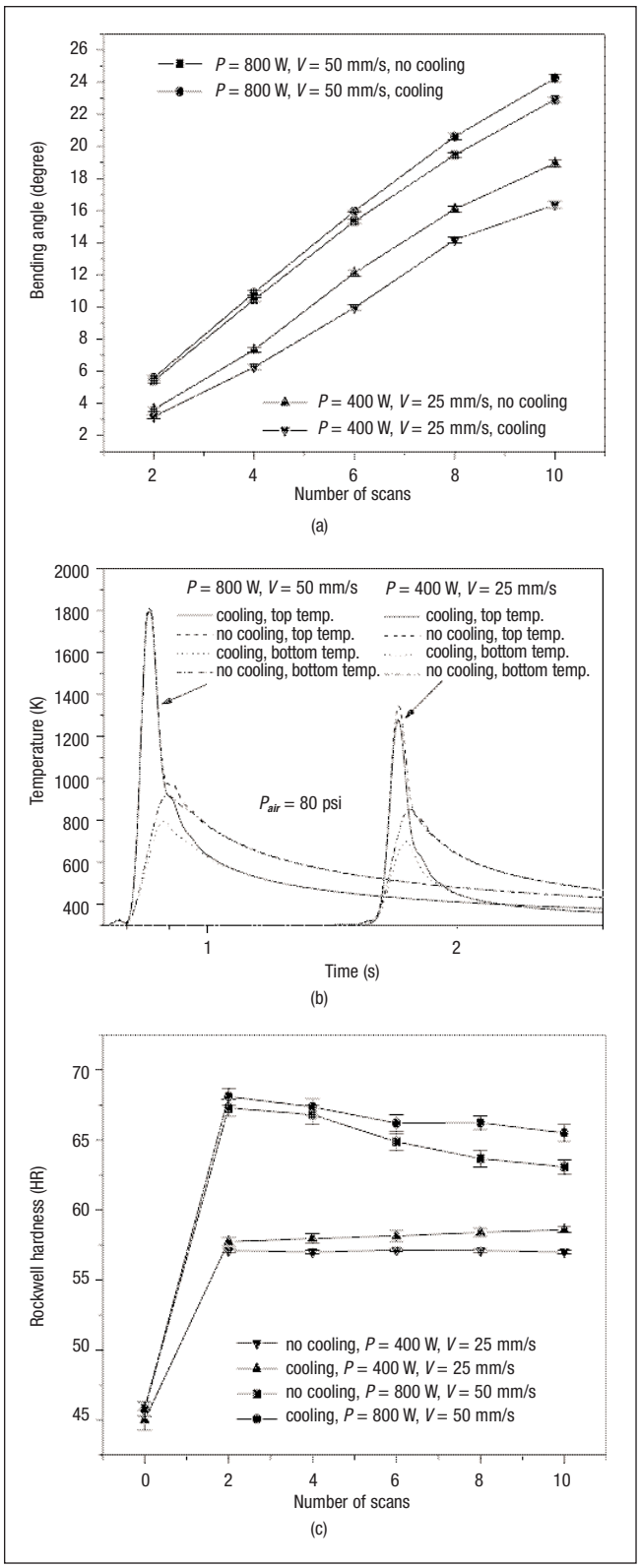

Figure 10
(a) Development of bend angle vs. number of scans, (b) temperature history of a single scan with cooling and without cooling, (c) Rockwell hardness vs. number of scans with cooling and without cooling (D_{beam} = 4 mm, P_{air} = 80 psi, δ = 0, bottom cooling only)

softening are about the same and as a result the hardness remains more or less constant while the number of scans increases.

Figures 8e and *8f* show the microstructure near the top and bottom surfaces after 10 passes of laser forming with cooling. For each pass in multiscan laser forming, the material experiences the phase transformation to austenite, then to ferrite, bainite, and a small amount of pearlite. The phase structure after 10 passes shows no visible difference from the phase structure after one pass.

Edge Effect

Figure 11a shows the numerical results of the bend angle variation along the scanning path under two conditions with and without cooling. The difference between the maximal and minimal bending angles along the scanning path is referred to as edge effect. As seen, the edge effect is reduced by about 54% and 17% for the two conditions, respectively, after cooling is applied. Similar results are also found under other conditions in this paper. This phenomenon can be explained by the numerical results shown in *Figure 11b*. The variation in the difference of *y*-axis plastic strain between the top and bottom surfaces is reduced with cooling. This is because cooling can reduce the heat-affected zone and the plastic zone, and therefore the accumulated plastic strain due to the bending taking place at the preceding regions along the scanning path is reduced.

The curvature of the bending edge is also decreased after the cooling bottom scheme is applied. The cause of the curved bending edge is due to the difference in *x*-axis contraction between the top and bottom surfaces.[12] *Figure 11c* shows that the difference in *x*-axis contraction between the top and bottom surfaces with cooling is lower than without cooling.

Cooling Scheme

Figure 12 compares the bending angle with cooling the bottom surface, cooling the top surface, and cooling both the top and bottom surfaces. The no-cooling case is also plotted as a benchmark. The total air pressure is 80 psi for all the cooling conditions. When both the top and bottom surfaces are cooled simultaneously, 40 psi of air pressure is used for each surface.

Among the three cooling schemes, the bottom-cooling scheme produces the largest bending angle while the top-cooling scheme produces the smallest.

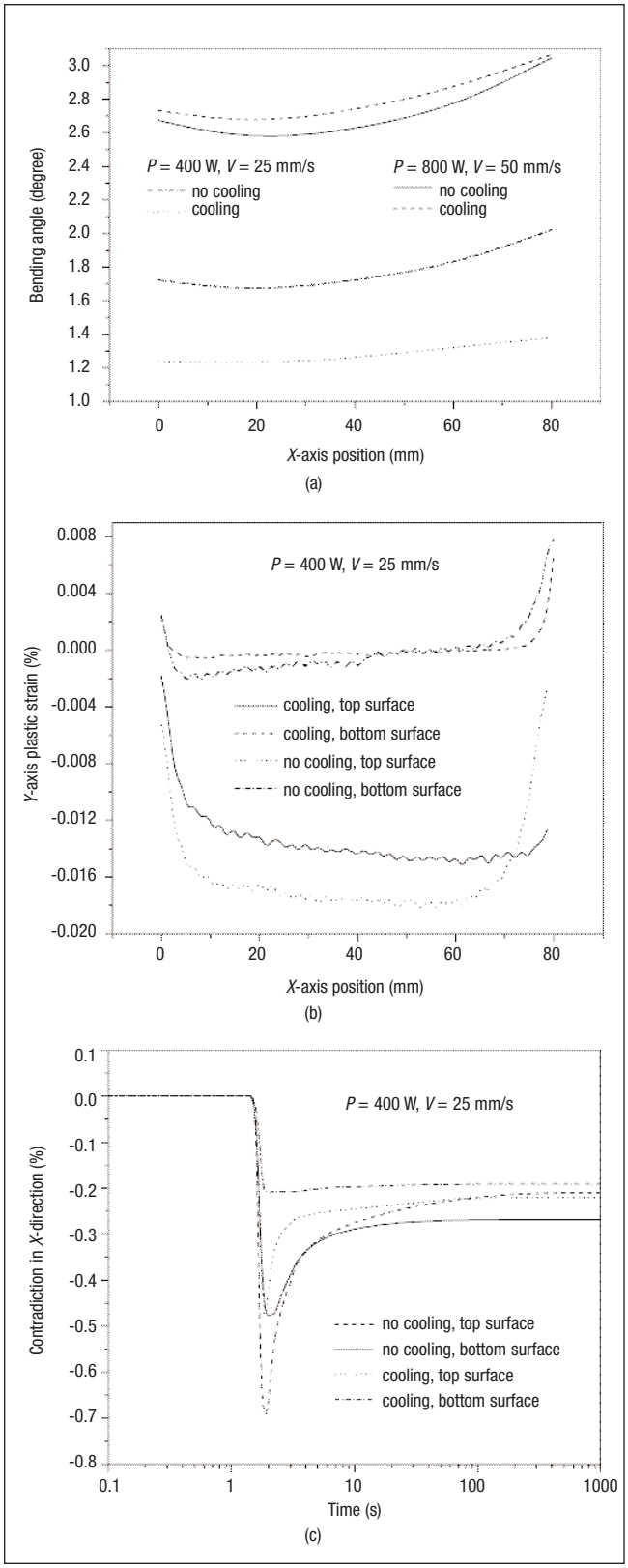

Figure 11
(a) Bend angle variation along scanning path, (b) *Y*-axis plastic strain along the scanning path, (c) Time history of *X*-axis contraction (D_{beam} = 4 mm, P_{air} = 80 psi, δ = 0, bottom cooling only)

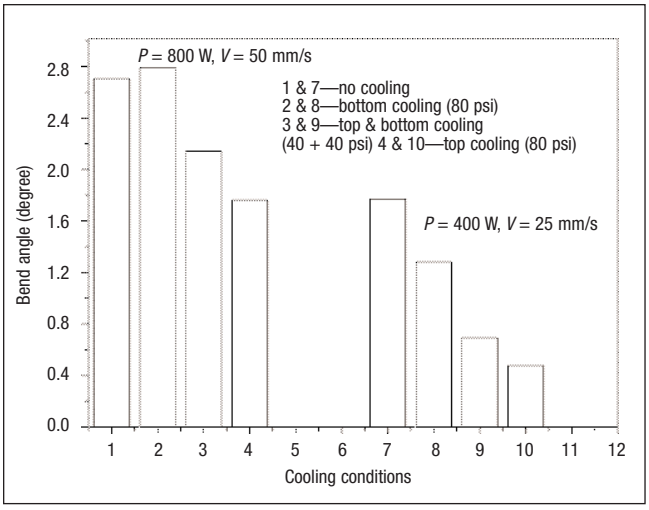

Figure 12
Comparison of Bend Angle Under Different Cooling Schemes (no cooling also included) (D_{beam} = 4 mm, δ = 0)

The bottom-cooling scheme reduces the temperature at the bottom surface and therefore increases the temperature gradient between the top and bottom surfaces. As a result, the bending angle is larger. Contrarily, the top-cooling scheme reduces the top-surface temperature and therefore reduces the temperature gradient between the top and bottom surfaces. As a result, the bending angle is smaller. The top and bottom cooling scheme is somewhere in between. In summary, the bottom-cooling scheme is most effective in terms of bending. But in terms of removing heat, the other two schemes should be favored because they cool the top surfaces where the temperature is the highest.

Buckling Mechanism

So far, the discussion has been focused on the cooling effects in laser forming where the temperature gradient mechanism (TGM) dominates. Laser forming can also be affected by the so-called buckling mechanism (BM), where the laser beam diameter is large compared with workpiece thickness. *Figure 13* shows the experimental results of BM-dominated laser forming using various cooling schemes. The experimental conditions are the same as in *Figure 12* except the beam diameter increases from 4 to 8 mm here.

First of all, the bending angle under any cooling scheme is smaller than that without cooling. This is understandable because in a BM-dominated laser forming process, the temperature gradient in the depth direction is small and the forming is achieved

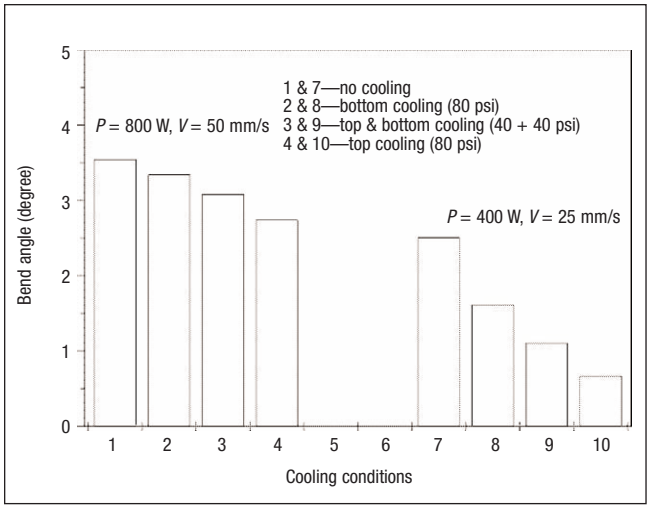

Figure 13
Comparison of Bend Angle by Different Cooling Schemes When Buckling Mechanism Dominates (no cooling also included) (D_{beam} = 8 mm, P_{air} = 80 psi, δ = 0)

through buckling induced by compressive strain that is almost uniform throughout the depth direction. Any efforts to reduce this uniformity, or in other words to increase the temperature gradient through cooling, are against the buckling mechanism.

It is seen that among the three cooling schemes, the bottom-cooling scheme continues to produce the largest bending angle, while the top-cooling scheme produces the smallest. The heat removal rate with bottom cooling is less than with top cooling. Therefore, the average temperature with bottom cooling is higher than with top cooling. When BM dominates, the bend angle increases as the average temperature increases. In addition, the cooling effect on flow stress increase is the largest with top cooling. Therefore, of the three cooling schemes, the bend angle with cooling the bottom surface is the largest, while cooling the top surface gives the smallest.

Conclusions

The cooling effect on forming efficiency varies with process conditions, and the variation is discussed in terms of the competing effect on temperature and flow stress by the cooling. The forming efficiency is also experimentally and numerically investigated in terms of nozzle offset and cooling air pressure, and numerical results agree with experimental results.

Cooling significantly reduces the total forming time in multiscan laser forming by greatly reducing the need for waiting time between consecutive scans. Multiscan is necessary if laser forming is to become a practical production process. Cooling only moderately decreases material ductility even after multiscan because the repeated work hardening is offset by repeated softening. The softening is obtained through recovery and recrystallization accompanying each scan. Grain refinement and partial phase transformation to bainite are also observed.

Acknowledgment

Support for this project under a NSF grant (DMI-0000081) is gratefully acknowledged. Dr. Wayne Li's assistance in numerical study and experiments in particular is also greatly appreciated.

References

1. A. Sprenger, F. Vollertsen, W.M. Steen, and K. Watkins, "Influence of Strain Hardening on Laser Bending," *Proc.* of Laser Assisted Net Shape Engg. (LANE '94) (v1, 1994), pp361-370.

2. K.U. Odumodu and S. Das, "Forceless Forming with Laser," ASME Materials Div. publication MD v74, 1996, pp169-170.

3. T.D. Hennige and M. Geiger, "Cooling Effects in Laser Forming," *Technical Papers of NAMRI/SME* (1999), pp25-30.

4. V. Olden, A. Smabrekke, and M. Raudensky, "Numerical Simulation of Transient Cooling of Hot Rolled Asymmetrical Ship Profile (Holland Profile)," *Ironmaking and Steelmaking* (v23, n1, 1996), pp88-91.

5. B. Debray, P. Teracher, and J.J. Jonas, "Simulation of the Hot Rolling and Accelerated Cooling of a C-Mn Ferrite-Bainite Strip Steel," *Metal. and Mat. Trans. A: Physical Metallurgy and Materials Science* (v26A, 1995), pp99-111.

6. M. Cristinacce and P.E. Reynolds, "Current Status of the Development and Use of Air Cooled Steels for the Automotive Industry," *Proc.* of 1996 Symp. on Fundamentals and Applications of Microalloying Forging Steels, 1996, pp29-43.

7. H. Martin, "Heat and Mass Transfer Between Impinging Gas Jets and Solid Surface," *Advances in Heat Transfer,* J.P Harnett and T.F. Irvine, eds., Vol. 13 (New York: Academic Press, 1977), pp1-60.

8. K.P. Perry, "Heat Transfer by Convention from a Hot Gas Jet to a Plane Surface," *Proc. of the Institution of Mechanical Engineers* (v168, 1972), p775.

9. B.A. Boley and J.H. Weiner, *Theory of Thermal Stresses* (Dover Publications, 1997).

10. T.H. Courtney, 1990, *Mechanical Behavior of Materials,* ch. 7 (New York: McGraw-Hill Series in Materials Science and Engg., 1990).

11. R.E. Reed-Hill, *Physical Metallurgy Principles*, ch. 17 and 18, PWS-KENT Series in Mechanical Engineering (1973).

12. J. Bao and Y.L. Yao, "Analysis and Predication of Edge Effects in Laser Bending," *Proc.* of 18th Int'l Congress on Applications of Lasers and Electro-Optics (ICALEO '99): Conf. on Laser Materials Processing, San Diego, CA, Section C, 1999, pp186-195.

Authors' Biographies

Mr. Jin Cheng is a PhD candidate and Dr. Y. Lawrence Yao is an associate professor at Columbia University. Dr. Yao's research interests are in manufacturing and design, laser machining, laser forming, and laser shock processing.